TITLE PAGE

How do alterations in root cap structure and integrity impact root responses to an increase in medium strength?

J. Roué, H. Chauvet, E. Badel, F. Bizet, B. Moulia, and V. Legué

Université Clermont Auvergne, INRA, PIAF, F-63000 Clermont–Ferrand, France

Juliette Roué - juliette.roue@uca.fr

Hugo Chauvet - hugo.chauvet-thiry@inra.fr

Eric Badel - eric.badel@inra.fr

François Bizet - fr_bizet@yahoo.fr

Bruno Moulia - bruno.moulia@inra.fr

Corresponding author: valerie.legue@uca.fr, (+33) 0 473405273

Date of submission: 07/27/2018

Number of tables: 1

Number of figures: 7

Word count: 6588

Supplementary data:

Number of tables: 0

Number of figures: 2

Videos: 6

How do alterations in root cap structure and integrity impact root responses to an increase in medium strength?

J. Roué, H. Chauvet, E. Badel, F. Bizet, B. Moulia, and V. Legué

Running title: root responses to an increase in growth medium strength

Highlight: The analysis of growth and orientation of *Arabidopsis thaliana* mutant roots affected in root cap structure showed that intact root cap layers are required to trigger the root responses to medium strength.

Abstract

During root progression in soil, root cap cells are the first to encounter obstacles. The root cap is known to sense environmental cues, making it a relevant candidate for a mechanosensing site. An original two-layer medium was developed in order to study root responses to growth medium strength and the importance of the root cap in the establishment of these responses. Root growth and trajectory of primary roots of *Arabidopsis thaliana* seedlings were investigated using *in vivo* image analysis. After contact with the harder layer, the root either penetrated it or underwent rapid curvature, allowing the reorientation of the root primary growth. The role of the root cap in penetration and reorientation was investigated by analyzing mechanically the responses of *Arabidopsis* mutant roots with altered caps. The primary root of *fez-2* mutant lines, which has less root cap cell layers than wild-type roots, showed impaired penetration ability. Conversely, *smb-3* roots of mutant lines, which display a higher number of root cap cells, showed enhanced penetration abilities. This work highlights that alterations in root cap structure affect the root responses to medium strength.

Key words: curvature, medium strength, Phytagel medium, root growth, root biomechanics, root buckling, root cap

Abbreviations: COL, columella; LRC, Lateral Root Cap; SI, Sharpness Index; SMB, SOMBRERO

Introduction

Roots grow in a complex soil environment, which exhibits spatial and temporal heterogeneities, arising from sand particles, stones or hardpans of soil that constitute physical obstacles. The ability of roots to penetrate the soil and to overcome physical obstacles depends either on their ability to find a path of least resistance, or on their ability to generate sufficient force to go through the obstacle (Bengough *et al.*, 2009; Vollsnes *et al.*, 2010; Colombi *et al.*, 2017*a*). The force needed to penetrate a soil, provided by root growth, is determined by the soil strength. In natural conditions, soil strength – commonly estimated by penetrometer measurements – is in the range of 1MPa (Jin *et al.*, 2013; Kolb *et al.*, 2017). Soil heterogeneities may be overcome with soil compaction or soil drying, which results in an increase of soil strength.

In a few studies carried out in laboratories, changes in soil strength have been mimicked with simplified models appropriate to studying root responses. The elaboration of a two-layer Phytagel-based growth medium, containing two layers of distinct Phytagel concentrations, enables the roots to experience variations in medium strength when penetrating from one medium layer to another (Yamamoto *et al.*, 2008; Yan *et al.*, 2017). It has been shown that adjusting the Phytagel concentration regulated the strength of the growth medium (Schiavi *et al.*, 2016). In two-layer media experiments, where roots faced a compliant layer and a stiff layer consecutively, root tips were submitted to an increasing axial stress as they encountered the interface between the two layers. Roots which did not manage to generate sufficient force to penetrate the lower layer underwent buckling, dramatically changing the root growth trajectory and the root straightness (Massa and Gilroy, 2003; Silverberg *et al.*, 2012; Bizet *et al.*, 2016). The maximal axial force a root is able to exert before buckling, given by Euler's law, depends on the rigidity, the length of the growth zone, and the diameter of the root to the 4th power (Kolb *et al.*, 2017). In accordance with Euler's law, species with a higher increase in root diameter and/or decrease in root elongation in response to medium strength are more efficient in penetrating strong layers (Materechera *et al.*, 1992). Besides root diameter and growth zone length, it has been shown that root tip geometry was also an important feature modulating root response to medium strength (Ruiz *et al.*, 2016; Colombi *et al.*, 2017*b*). In compacted soils,

74 root tips with an acute opening angle grow faster than root tips with a blunted geometry (Iijima
75 *et al.*, 2003*a*,*b*; Colombi *et al.*, 2017*b*). Colombi et *al.* (2017) showed that the root tip shape
76 influenced the penetration stress experienced by roots, by modulating the distribution of the
77 local compaction concentrated around the tip.

78 The shape of root tips arises from the shape of the root cap that covers and protects the root
79 apical meristem. The root cap is composed of the Columella (COL) located at the center of the
80 root cap and the Lateral Root Cap (LRC) (Arnaud *et al.*, 2010; Kumpf and Nowack, 2015). In
81 *Arabidopsis thaliana*, the mature COL and LRC are organized in 3 to 5 cell layers of increasing
82 age. Every formative division of root cap stem cells generates a new differentiating cell layer
83 which pushes the older root cap layers towards the root periphery. COL mature cells are known
84 to sense gravity, thanks to the amyloplasts they contain, conferring to the root cap the ability
85 to trigger tropisms in the root (Sato *et al.*, 2015). LRC mature cells principally act as secretory
86 cells which synthesize and export high molecular weight polysaccharide mucilage (Kumpf and
87 Nowack, 2015). Once mature, COL and LRC cell layers reach the periphery of the root cap
88 where they end up being sloughed off, allowing the root cap to keep a determinate, constant
89 size (Barlow, 2003). The balance between cell production and cell sloughing controls the root
90 tip shape. The study of root cap formation allowed the identification of the molecular actors
91 involved in cell production, differentiation and sloughing. Among these actors, FEZ and
92 SOMBRERO (SMB) transcription factors of the NAC family [NAM (NO APICAL MERISTEM), ATAF
93 (*ARABIDOPSIS* TRANSCRIPTION ACTIVATION FACTOR) and CUC (CUP-SHAPED COTYLEDON)]
94 were identified. FEZ specifically promotes periclinal divisions of COL and LRC stem cells
95 (Willemsen *et al.*, 2008). The *fez-2* mutant, resulting from the loss of function of *FEZ*, exhibits a
96 lower rate of periclinal division of the root cap stem cells which leads to the reduction of COL
97 and LRC cell layers compared to wild-type roots (Willemsen *et al.*, 2008; Bennett *et al.*, 2014).
98 SMB prevents the division of the differentiating root cap daughter cells and promotes their
99 differentiation. Additional COL and LRC cell layers are observed in the *smb-3* loss-of-function
100 mutant and the outer LRC cell layer reaches the end of the elongation zone (Willemsen *et al.*,
101 2008; Bennett *et al.*, 2010).

102 The objective of our study is to understand whether the structure of the root cap, controlled by
103 root cap integrity, is required in the establishment of root response to medium strength. We
104 hypothesized that the shape of the root cap could alter root responses in relation to an
105 increase in medium strength, with pointed caps facilitating root penetration and blunted or
106 domed caps complicating root penetration. We chose to study the root response to medium
107 strength through the *fez-2* and *smb-3 Arabidopsis thaliana* mutant lines. We characterized the
108 root tip geometry of *fez-2* and *smb-3* mutants precisely to understand whether the loss or the
109 gain of root cap cell layers impacted root tip shape. Then, the mutants were studied using a
110 novel experimental set-up which allows the quantitative imaging of the growth and the
111 orientation of the root. We cultivated Col-0, *fez-2* and *smb-3* roots in a two-layer Phytagel
112 medium of increasing mechanical resistance. Using a spatiotemporal analysis, we characterized
113 the penetration ratio, the root growth rate, and the root curvature of wild-type and mutant
114 roots from the upper layer to the lower layer. This simple experimental method allowed us to
115 describe three distinct root reorientations in response to increases in medium strength. We
116 discovered that the penetration ability and the reorientation in *fez-2* and *smb-3* were affected
117 in exactly the opposite way to what was hypothesized. Our results suggest that shape does not
118 seem to be the key feature influencing root response to medium strength.

119 **Material and Methods**

120 **Plant growth medium**

121 For all of the experiments, we used Phytagel as a substitute for Agar in the *in vitro* growth
122 medium. Phytagel is preferentially chosen for its higher temperature stability, higher
123 mechanical strength and better optical clarity (Schiavi et al., 2016). The growth medium
124 consisted of half-strength Murashige and Skoog (MS/2) medium adjusted to pH 5.7 and
125 containing Phytagel at different concentrations. The two-layer media consisted in the
126 superposition of an upper layer of growth medium containing 0.2% (w/v) of Phytagel and a
127 lower medium layer containing 0.2 % (w/v), 0.3% (w/v) or 0.5 % (w/v), called 0.2-0.2, 0.2-0.3
128 and 0.2-0.5 respectively (Fig. S1). The two-layer media were poured into specific culture
129 chambers which consisted in Polycarbonate boxes of 100 X 20 mm, and 60 mm height which

130 allowed root seedlings to grow vertically inside the growth medium. The two-layer media were
131 prepared as follows: 60 mL of sterilized MS/2 medium containing 0.2 % (w/v), 0.3% (w/v) or 0.5
132 % (w/v) of Phytagel were poured into the culture chambers under aseptic conditions, then,
133 these were rapidly closed and placed on ice. After 10 min, 20 mL of a sterilized MS/2 medium
134 containing 0.2 % (w/v) of Phytagel were poured over the lower medium layer.

135 **Plant material**

136 The wild-type strain of *Arabidopsis thaliana* (ecotype Columbia, Col-0) and *fez-2*, *smb-3*
137 *Arabidopsis thaliana* null-mutants used for the experiments were provided by B. Scheres's
138 laboratory (Willemsen *et al.*, 2008; Bennett *et al.*, 2010, 2014). The seeds were surface
139 sterilized with 30% (v/v) sodium hypochlorite solution, added to 2% (v/v) Triton X-100 for 10
140 min. After 5 washes in sterile distilled water, 10 seeds were gently placed on the surface of the
141 upper layer of the MS/2 two-layer medium. After sowing, the culture chambers were sealed
142 and kept at 4 °C in the dark for 2 days. Then, they were placed at 23 °C under a 16 h-
143 photoperiod.

144 **Mechanical properties of Phytagel growth medium**

145 To measure the mechanical properties of each concentration of the Phytagel medium,
146 compressive and penetration tests were performed, allowing the determination of the elastic
147 modulus and the mechanical penetration resistance of the media, respectively.

148 *Determination of elastic modulus*

149 Growth media containing from 0.2% to 1.2% (w/v) of Phytagel were poured into Petri dishes
150 having a thickness of 10 mm. 20x20x10 mm^3 Phytagel cubes were then cut and placed in the
151 Instron device (Tensile testing machine, Instron 5565). An uniaxial compression was applied on
152 the surface of the gels by the displacement of an upper plate with a constant loading rate of 0.5
153 $mm.min^{-1}$. A 100 N load cell recorded the force needed to deform the samples. Real-time load-
154 displacement data of each sample were exported by Console Bluehill 2 software and provided
155 characteristic stress-strain curves (Fig. 1A, B). After a typical contact step, the loading force
156 increased with the compression rate of the sample, before decreasing notably with the slipping

157 or the rupture of the sample. In the linear portion of the curve, *i.e.* when stress is proportional
158 to strain, the deformation is considered to be elastic (Schiavi *et al.*, 2016). The elastic modulus
159 (E) values of the Phytagel samples were determined from the ratio between the incremental
160 stress Δσ and the incremental strain rate Δε during elastic deformation by applying the Hooke's
161 law:

162 $$E = \frac{\Delta\sigma}{\Delta\varepsilon},$$

163 Where

$$\sigma = \frac{F}{A},$$

$$\varepsilon = \frac{l0}{\Delta \mathrm{l}},$$

164

165 and F is the compression force (N), A is the surface area of the cross section of the sample (m^2)
166 on which the force is applied, l_0 is the initial thickness of the sample (m), Δl is the variation of
167 this thickness, *i.e.* the displacement of the plate (m). Compressive tests were conducted in 3
168 samples for each Phytagel concentration.

169 *Determination of penetration resistance*

170 Penetration tests were conducted in 0.2-0.2, 0.2-0.3 and 0.2-0.5 two-layer media. The samples
171 of the Phytagel medium were prepared as described above. A 2.5 mm diameter needle was
172 attached to a load cell (Instron, 100 N max) and driven downward through the growth medium
173 at a rate of 1 $mm.min^{-1}$. The real-time data were exported by Console Bluehill 2. The maximal
174 force required for the rupture of the surface of the lower layer was measured.

175 **Time lapse photography and image processing**

176 Root growth and orientation were time-lapsed 5 days after sowing. Two Nikon D7100 cameras
177 equipped with macro lenses (AF-S micro NIKKOR 60mm f/2.8G ED) and controlled by
178 DigiCamControl software, were placed on a rack in front of the culture chambers. Images of the
179 roots growing in the two-layer medium were acquired every 5 min during the period of the
180 experiment. All photographs were pre-treated using Rawtherapee software (v4.2.1) and were

181 then analyzed using a software developed by our laboratory, named RootStem Extractor. The
182 principle and procedures of the software were described in Chauvet *et al.* (2016). Briefly, the
183 software allowed the extraction of the topological skeleton of each root by screening pictures
184 perpendicularly to the root axis with a step of 0.3 pixel. The length of the root on each picture
185 and the local inclination as a function of the curvilinear abscissa can be computed from the
186 coordinates of the skeleton. The root length, as a function of time, allowed us to calculate the
187 root growth rate by the means of linear fit. By deriving the local inclination as a function of time
188 and space, curvature intensity along the root could be obtained. For each root, the curvature
189 intensity data are presented in a graph composed of 3 dimensions: a vertical axis corresponding
190 to root length from the beginning of the measurement, a horizontal axis corresponding to time
191 and a color bar representing the intensity of curvature.

192 **Root tip geometry and determination of Sharpness Index**

193 The root tips of Col-0, *fez-2* and *smb-3 Arabidopsis thaliana* lines were stained with a pseudo-
194 Schiff propidium iodide staining technique, as described in Truernit *et al.* (2008). They were
195 deposited between the slide and the cover slip and observed with a Zeiss LSM 800 laser
196 scanning microscope (Carl Zeiss Microscopy) coupled to a Apochromat X20 objective. From
197 longitudinal root observations, pictures of the longitudinal median section from the quiescent
198 center to the extremity of the root cap were extracted for each genotype. The area of the radial
199 section of the root tip was calculated using ImageJ software (v1.52d, http://imagej.nih.gov/ij/).
200 The vertical axis L_R and the radius of the root at the quiescent center R_R were measured (Fig.
201 2D1). We evaluated the Sharpness Index (SI) of the root tip according to the following equation
202 (Fig. 2D2):

$$SI = \frac{A_R - (L_R * 2R_R)/2}{L_R * 2R_R - (L_R * 2R_R)/2}$$

203 Where, A_R is the area of the root. The closer *SI* is to 0, the more the root tip is pointed.
204 However, the closer *SI* is to 1, the more the root tip has a rectangular shape.

205 **Maximal root growth forces**

206 The maximal forces roots were able to exert before buckling were estimated for Col-0, *fez-2*
207 and *smb-3* roots grown in 0.2-0.3 medium. After contact between the root tip and the lower
208 layer surface, the root tips deformed the lower medium until root deflection or root tip
209 deviation. The shape of the lower layer surface just before buckling was traced using ImageJ
210 software and the displacement (*d*) of the surface towards its initial position was measured (Fig.
211 4A). The shape of the root tip extremity was fitted by a circle of radius *R*. The maximal force
212 before root buckling F_{crit} applied on the surface by the root tip was then estimated using the
213 theory of contact between a sphere and a half-space (Hanaor *et al.*, 2015),

$$F_{crit} = \frac{4}{3}\, E^{*}\, R^{\frac{1}{2}}\, d^{\frac{3}{2}}$$

214 where

$$\frac{1}{E^{*}} = \frac{1-\nu_1^2}{E_1} + \frac{1-\nu_2^2}{E_2}$$

215 and *E1, E2* are the elastic moduli of the lower medium layer and of the root tip respectively,
216 and *v1, v2* are the Poisson's ratios of the lower layer and the root tip respectively. To calculate
217 E^{*}, we assumed that E_2 was very close to E_1, allowing us to neglect the second part of the
218 formula. Moreover, according to the literature, *v1* is estimated at 0.5 (Ahearne *et al.*, 2005).

219 **Statistical analysis**

220 All data were statistically analyzed using R software (Rstudio, R.3.3.4, https://www.r-
221 project.org/). The Shapiro-Wilk test was used to test for normal distribution of the data and the
222 Bartlett test was used to test for homoscedasticity. One-way Analysis of Variance (ANOVA) or
223 two-way ANOVA were applied on the data, to determine whether the effect of each factor was
224 significant. When significant differences were obtained, post-hoc analyses based on the Tukey
225 test were applied on the data.

226 **Results**

227 **Phytagel concentration in the medium impacts both medium rigidity and penetration**
228 **resistance**

229 The elastic modulus E, obtained from the stress-strain measurements, was calculated for the
230 Phytagel concentrations ranging from 0.2 to 1.2% (Fig. 1A, B). The curve showed that E was
231 highly dependent on the concentration of Phytagel and that this dependence was nonlinear
232 (Fig. 1C). The 0.2%, 0.3%, 0.5% and 1.2% Phytagel growth medium showed E values of 3.07 ±
233 0.13 kPa, 7.60 ± 0.79 kPa, 31.93 ± 3.81 kPa and 158.30 ± 10.59 kPa, respectively (Fig. 1C).

234 Penetrometer assays were realized in 0.2-0.2, 0.2-0.3 and 0.2-0.5 two-layer media (Fig. 1D, E).
235 The curves of the compression force as a function of the needle displacement revealed the
236 same pattern for all of the growth media analyzed. The compression force increased markedly
237 as the needle deformed the surface of the lower medium layer until a breaking point after
238 which the loading force again became weak (Fig. 1E). The breaking point indicates the rupture
239 of the lower layer surface and the penetration of the needle into the lower layer. The curves
240 illustrate the presence of an interface between the two medium layers, whose rupture requires
241 a specific force depending on the Phytagel concentration (Fig. 1E). The rupture of the 0.2%
242 lower layer surface was induced by a force of 0.032 ± 0.004 N (Fig. 1F). The force required to
243 break the 0.3% lower layer surface was of 0.054 ± 0.008 N and the force required to break the
244 0.5% lower layer surface was of 0.11 ± 0.009 N (Fig. 1F). The data obtained from the
245 penetration tests showed that the strength of the interface increases significantly with the
246 Phytagel concentration of the lower medium layer (Fig. 1F). The 0.2% layer surface was
247 considered as the most brittle, the 0.5% surface as the strongest and the 0.3% surface as the
248 middle-strength medium. The mechanical measurements illustrated a great regularity and
249 repeatability for each Phytagel concentration, suggesting a stable behavior and good
250 homogeneity of the Phytagel media.

251 In conclusion, the determination of Elastic modulus and penetration resistance allowed the
252 characterization of the mechanical properties of the Phytagel media used for our experiments.
253 An increase in the concentration of Phytagel in the medium generated increases in both
254 medium rigidity and penetration resistance.

255 ***fez-2* and *smb-3 Arabidopsis thaliana* mutants exhibit an altered root cap shape**

256 Alterations in root cap cell layer number, cell division and differentiation in *fez-2* and *smb-3*
257 loss-of-function mutants have been precisely detailed (Willemsen *et al.*, 2008; Bennett *et al.*,
258 2010, 2014) and seem to have consequences on root tip shape. In this regard, it was important
259 to estimate this impact on each of the mutant lines studied. The reduction of COL and LRC cell
260 layers associated with the loss of function of *FEZ*, led to a shorter root cap narrower at the
261 base, compared to the wild-type (Fig. 2A, B, E). The estimation of the Sharpness Index (SI), of
262 0.30 ± 0.03 in *fez-2* roots and of 0.41 ± 0.03 in wild-type roots, showed that *fez-2* roots tips
263 were significantly more pointed than those of the wild-type ones (Fig. 2F). On the contrary, the
264 additional COL and LRC cell layers observed in the *smb-3* mutant, led to an increase in root
265 diameter at the quiescent center (Fig. 2C, E). The SI of the *smb-3* root tips was around 0.5 ±
266 0.02, illustrating their dome shape (Fig. 2F). The mean root diameter, measured at 500 µm from
267 the root tip, was not significantly different between *fez-2, smb-3* and wild-type roots,
268 suggesting that the mutations only impact the cap size (Fig. 2E). The analysis of the root growth
269 in the 0.2% one-layer Phytagel growth medium showed that the mean growth rate of wild-type
270 (3.10 ± 0.21 $\mu m.min^{-1}$) and *fez-2* (2.97 ± 0.18 $\mu m.min^{-1}$) roots was not significantly different (Fig.
271 2G), whereas *smb-3* roots grew much more slowly, with a mean rate of 1.65 ± 0.08 $\mu m.min^{-1}$
272 (Fig. 2G). Our characterization corroborates the analyses made by Bennett et al. (2010, 2014)
273 and the distinct phenotypes of the two mutant lines will allow the study of the role of root cap
274 shape in root responses to medium strength.

275 **The medium strength impacts both the penetration ability and the growth rate of *Arabidopsis***
276 ***thaliana* primary roots**

277 The penetration ability of *Arabidopsis thaliana* wild-type roots was observed in the 0.2-0.2, 0.2-
278 0.3 and 0.2-0.5 two-layer media (Table 1, Fig. S1). In the 0.2-0.2 medium, 100% of wild-type
279 roots progressed in the 0.2% upper layer, and crossed the interface to penetrate the 0.2%
280 lower layer. The analysis of root growth rate showed that only a short-term decrease in root
281 growth rate was observed 2 hours after contact (Fig. 3A). This slight decrease was followed by
282 the recovery of the initial root growth rate (Fig. 3A and Fig. 2G, 3$\mu m.min^{-1}$). The moment of

283 growth rate recovery corresponded to the rupture of the lower layer surface. One
284 representative example of *Arabidopsis thaliana* wild-type root penetration into the 0.2% lower
285 layer is presented in 3D graph (Fig. 5D), illustrating the impact of root penetration on root
286 growth rate and root straightness. On the graph, the increase in root length, as a function of
287 time, was linear before and after contact with the lower layer surface and confirmed the
288 transient impact of the root progression across the interface on root growth. The curvature
289 intensity was illustrated by the colors with the green indicating straight zones of the root. The
290 curvature intensity, along the penetrating root, lied between -1 and 1 mm^{-1}, illustrating root tip
291 oscillations around the vertical position during its growth (Fig. 5D). Right after contact, a zone
292 of slight curvature with an intensity below 2 mm^{-1} was initiated, represented by the horizontal
293 yellow strip on the graph. In the 0.2-0.3 two-layer medium, 60% of the *Arabidopsis thaliana*
294 primary roots penetrated the lower layer (Table 1). In parallel, the growth rate of penetrating
295 roots decreased by 30% within the first 30 minutes after contact with the lower layer surface
296 and recovered the initial growth rate within 300 minutes (Fig. 3D). The recovery of the initial
297 growth rate occurred after surface rupture and root penetration into the lower medium layer.
298 For some of the *Arabidopsis thaliana* penetrating roots, the decrease in the growth rate was
299 accompanied by the induction of a slight zone of curvature (data not shown). In the 0.2-0.5
300 two-layer medium, none of the *Arabidopsis thaliana* roots penetrated the lower layer (Table 1).

301 In conclusion, our results illustrated that the strength of the lower layer surface impacts the
302 penetration ability of *Arabidopsis thaliana* roots and affects their growth rate.

303 **The root penetration ability is impaired in *fez-2* roots and enhanced in *smb-3* roots**

304 To understand the role of root cap shape in response to medium strength, the penetration
305 abilities of *fez-2* and *smb-3* roots were compared to those of wild-type roots in 0.2-0.2, 0.2-0.3
306 and 0.2-0.5 two-layer media. All of the *smb-3* roots penetrated the 0.2% lower layer whereas
307 83% of the *fez-2* roots penetrated it (Table 1). The root growth rate of the mutant lines, 3.2
308 $\mu m.min^{-1}$ for *fez-2* and 1.5 $\mu m.min^{-1}$ for *smb-3*, was not significantly affected during root
309 penetration into the lower medium layer and corresponded to the initial root growth rate
310 observed in the 0.2% one-layer medium (Fig. 2G and Fig. 3B-C). Root penetration into the 0.3%

311 Phytagel lower layer was observed for 28% of the *fez-2* roots and 80% of the *smb-3* roots (Table
312 1). The root growth rate of *fez-2* and *smb-3* decreased by approximately 10% after root
313 penetration into the lower layer (Fig. 3E-F). In the 0.2-0.5 medium, only the *smb-3* roots
314 managed to penetrate the lower layer, with a penetration ratio of 18% (Table 1).

315 Thus, the *fez-2* roots exhibited an impaired penetration ability in response to mechanical
316 strength, whereas the *smb-3* roots exhibited an enhanced penetration ability. The root
317 penetration ratios revealed a variable ability of roots of a same genotype to face a given
318 mechanical resistance. To go further, the critical force that each root was able to exert before
319 reorienting was estimated.

320 **Critical force of wild-type, *fez-2* and *smb-3* roots facing an increase in medium strength**

321 To measure the critical force of wild-type (Col-0), *fez-2* and *smb-3* roots, the shape of the 0.3%
322 lower layer surface of elastic modulus E = 7.6 kPa was traced for each root just before root
323 curvature initiation (Fig. 4A). Wild-type roots displaced the surface at a mean maximal depth *d*
324 of 0.37 ± 0.03 mm, the *fez-2* roots displaced it at a mean *d* of 0.27 ± 0.01 mm and the *smb-3*
325 roots displaced it at a mean *d* of 0.49 ± 0.03 mm (Fig. 4B). The critical force was estimated
326 thanks to the values of *d*, of the radius of root tips and of the rigidity of the lower medium
327 layer. The mean critical force was estimated at 1.12 ± 0.14 10^{-9} N for wild-type roots, 0.66 ±
328 0.07 10^{-9} for *fez-2* N roots and 1.77 ± 0.18 10^{-9} N for *smb-3* roots, confirming that *smb-3* roots
329 were able to exert the highest force before curving while *fez-2* roots curved sooner (Fig. 4C).

330 ***Arabidopsis thaliana* primary roots exhibit distinct curvature establishments in response to**
331 **an increase in medium strength**

332 Representative examples of wild-type roots facing 0.3% and 0.5% lower layers are presented on
333 a spatiotemporal graph (Fig. 5, Fig. S3, Fig. S4). Following the contact with the 0.3% lower layer
334 surface, non-penetrating roots firstly grew downward against the surface and deformed it
335 without breaking it (Fig. 5B). A significant decrease in the root growth rate was observed (Fig.
336 5E). Within 2 h to 4 h after contact, a zone of curvature, illustrated by the red patch, was
337 observed at 500 µm to 1 mm from the root tip extremity. As roots continued to grow

338 downward, a second curvature zone, represented by the blue patch, appeared 3 h to 5 h after
339 the first one. The two curvatures exhibited a maximal intensity of 5 mm^{-1} (Fig. 3C). After their
340 formation, these zones of curvature were fixed in the root. Around 20 h after contact, the root
341 underwent a third curvature zone. This resulted in the deviation of the root tip axis allowing the
342 root tip to reorient its growth (Fig.5B). Root visualization in 2D did not allow the detailed
343 analysis of the third curvature. From now on, the term "curly phenotype" will be used to
344 describe roots drawing curls in response to lower layer surface strength.

345 In the 0.2-0.5 medium, the roots grew vertically against the stiff lower layer surface for 30 min
346 to 2 h after contact (Fig. 5C, F). The root growth rate decreased significantly within the first few
347 minutes following the contact with the lower layer surface (Fig. 5F). A first curvature was
348 established at approximately 400 µm from the root tip within 2 h following contact (Fig. S4).
349 The first curvature induced the deviation of the root tip, allowing the root to grow horizontally
350 along the surface of the lower layer. This first curvature exhibited a maximal intensity of 6 mm^{-1}
351 and was confined to its zone of formation. While the root tip reoriented its growth, a second
352 zone of curvature was formed at 300 µm from the root tip around one hour after the
353 establishment of the first curvature with a maximal intensity corresponding to 4 mm^{-1}(Fig. 5F).
354 Although the first curvature was fixed after its formation, the second one moved to stay at the
355 same distance from the root apex during root growth along the surface. During root
356 reorientation, no recovery of the initial growth rate was observed (Fig.S2). From now on, the
357 term "step-like phenotype" will be used to describe roots responding to the change in medium
358 strength in this way (Fig. S4).

359 **The *fez-2* and *smb-3* mutant roots exhibit altered curvature establishment**

360 The 20% of *fez-2* roots which did not penetrate the 0.2% lower layer exhibited the curly
361 phenotype (Fig. 6A, Fig.S5). The first curvature was initiated at 500 µm from the root apex and
362 exhibited a maximal intensity of 5 mm^{-1} (Fig. 6B). Root growth rate decreased rapidly and
363 notably after the contact with the lower layer surface. The *fez-2* root reorientation in the 0.2-
364 0.2 medium was very similar to wild-type root reorientation in the 0.2-0.3 medium (Fig. 5E and
365 Fig. 6B). The spatiotemporal analysis of deviation of *fez-2* root tips in the 0.2-0.3 and 0.2-0.5

366 media showed that *fez-2* non-penetrating roots had a step-like phenotype (Fig. 6C-F, Fig. S6,
367 Fig. S7). In both media, the first curvature was formed within 1 h following contact at around
368 500 µm from the root apex and the second curvature was formed right after, very close to the
369 root apex. The maximal intensity of the two curvatures was equal to 4 mm^{-1} in the 0.2-0.3
370 medium and to 2 mm^{-1} in the 0.2-0.5 medium, suggesting that the curvature intensity of *fez-2*
371 roots depends on the strength of the lower layer (Fig. 6D and F). The second curvature intensity
372 was very weak in step-like shaped *fez-2* roots compared to step-like wild-type roots. The root
373 growth rate of the step-like shaped *fez-2* roots was linear after contact and during root growth
374 reorientation (Fig. 6D and F).

375 In the 0.2-0.3 medium, *smb-3* non-penetrating roots exhibited the curly phenotype as observed
376 for wild-type roots (Fig. 7A). As *smb-3* roots grow much more slowly than other genotypes, the
377 curls were only initiated 6 h after the contact with the lower layer surface (Fig. 7B). The
378 maximal intensity of curvatures was close to 5 mm^{-1} (Fig. 7B). In the 0.2-0.5 medium, the *smb-3*
379 non-penetrating roots reoriented either by undergoing several deflections (Fig. 7C, Fig. S9), or
380 by establishing two curvatures (Fig. 7E). In the first case, the roots exhibited large waves with
381 maximal curvature intensities reaching 8 mm^{-1} (Fig. 7D). Moreover, the root growth rate of the
382 *smb-3* roots was unchanged during the formation of the waves (Fig. 7D). In the second case, the
383 two curvatures exhibited a similar maximal intensity of 5 mm^{-1}. The first and second curvatures
384 were initiated at 300 µm from the root apex (Fig. 7F). The second curvature intensity was
385 significantly higher than in wild-type roots. For these roots, the growth rate decreased slightly
386 after the contact with the lower layer surface (Fig. 7F, Fig. S2). As in wild-type roots, no
387 recovery of the initial root growth rate was observed after complete root reorientation (Fig.
388 S2).

389 **Discussion**

390 Our experimental set-up has proved insightful for understanding root responses to medium
391 strength. The precise characterization of media mechanical properties showed a strong
392 correlation between medium rigidity and penetration resistance. Moreover, the precise
393 spatiotemporal analysis of root growth rate and orientation allowed us to delve further into the

394 discrimination of passive and active mechanisms involved in root reorientation. The achieved
395 characterization of root reorientation led to a better understanding of the role of the root cap
396 in root responses to mechanical stresses.

397 **Root reorientation involves both passive and active mechanisms**

398 In our experimental system, roots grew through an upper medium layer of compliant strength
399 until encountering a lower layer, where penetration requires an increase in root growth
400 pressure. The contact between the wild-type root tip and the middle-strength and the
401 strongest lower layer surfaces led to a rapid decrease in root growth rate. This decrease,
402 observed for both penetrating and non-penetrating roots, was comparable to that observed in
403 poplar roots submitted to a physical obstacle, and may arise from the dedication of turgor
404 pressure to root penetration rather than to cell elongation (Bizet *et al.*, 2016). The root growth
405 against the lower layer surface creates a progressively increasing compression force on the root
406 (Kolb *et al.*, 2017). If the compression force reaches a critical value while the root is still in
407 contact with the obstacle, Euler's buckling can occur (Bizet *et al.*, 2016). We estimated that
408 non-penetrating wild-type roots supported a critical compression force of 1.12 10^{-9} N before
409 buckling. These forces are 10^{6} times less important than the critical buckling force measured on
410 Poplar adventitious roots (Bizet *et al.*, 2016). This difference may be explained by the difference
411 in root diameter between the two species and by the differences in root rigidity.

412 Buckling was observed for wild-type, *fez-2* and *smb-3* non-penetrating roots and led to
413 three distinct morphologies depending on the genotype and on the strength of the lower layer
414 surface. When encountering an intermediate medium strength, non-penetrating roots mostly
415 exhibited a curly-shape. This shape was already observed in *Medicago truncatula* roots growing
416 in a two-layer Phytagel media (Silverberg *et al.*, 2012). From a mathematical model based on
417 the theory of buckling rods, the authors assigned the curly morphology of M*edicago* roots to a
418 combination of helical buckling and simultaneous twisting near the root tip. Lateral
419 containment by the upper medium layer seemed to be a key feature modulating root helical
420 buckling (Silverberg *et al.*, 2012). Poplar roots grown in non-constraining hydroponic solution
421 and submitted to a physical obstacle buckled with a long wavelength curve shape (Bizet *et al.*,

422 2016). In our experimental system, some *smb-3* non-penetrating roots adopted this shape that
423 we called the wavy phenotype. In two-layer media, as all of the upper layers had the same
424 mechanical strength, the various shapes adopted by roots cannot be attributed to their
425 constriction level but more probably to their variability of anchorage or diameter. For most of
426 the curly-shaped and wavy-shaped roots, the first curvature was initiated and confined in a
427 zone between 400 and 500 µm from the root tip, corresponding to a zone of mechanical
428 weakness (Bizet *et al.*, 2016). All these observations suggest that curly and wavy phenotypes
429 are mainly driven by the mechanical response of the root acting as a "growing" rod blocked by
430 the obstacle.

431 The step-like phenotype was adopted by roots mostly in response to the highest increase in
432 medium strength. In this case, the first curvature induced the deviation of the root tip, which
433 implied a change in mechanical forces applied on the root tips from axial to asymmetric radial
434 forces. The rapidity and position of curvature initiation suggest that it may be interpreted as a
435 buckling. The first curvature was followed by the initiation of a second one, closer to the root
436 apex, allowing the root tip to regain the vertical position. This second curvature provided the
437 root tip with a steady form from changing cells, and was previously described as the result of
438 the interaction between gravitropic and thigmotropic responses (Massa and Gilroy, 2003). The
439 root tip deviation was preceded by a reduction in root growth rate which did not recover after
440 relaxation of axial mechanical stresses. The initiation of the second curvature and the
441 maintenance of the reduced root growth rate suggest that, even if the first curvature was
442 initially provoked by a buckling, the further root growth direction may be reoriented in an
443 active way.

444 The different patterns of curvature establishment suggest that the mechanical strength of the
445 lower layer surface determines the ensuing root response (buckling or bending). A middle-
446 strength medium surface allows the root tips to sink into it, preventing their deviation after
447 root buckling. On the contrary, a strong medium surface is barely deformed by the root tips,
448 which may be free to deviate and may trigger an active root reorientation.

449 **Root cap shape is not the key feature impacting root responses to an increase in medium**
450 **strength**

451 Based on previous studies (Vollsnes *et al.*, 2010; Ruiz *et al.*, 2016; Colombi *et al.*, 2017*b*), we
452 hypothesized that root cap shape, by changing the distribution of axial mechanical stresses
453 around the root tip, influenced root penetration ability and root response to medium strength.
454 It has been shown that a pointed root tip increased the concentration of axial stresses at the tip
455 forefront rather than around the tip, resulting in enhanced crack initiation and reduced
456 penetration stress. Contrary to what was expected, *fez-2* roots, with an acute tip, exhibited
457 reduced penetration abilities whereas *smb-3* roots, with a dome-shaped tip, exhibited
458 enhanced penetration abilities compared to wild-type roots. These conflicting results suggest
459 that root cap shape may not be the key feature determining root response to medium strength.
460 To confirm this, attention should be paid to the cap rigidity of wild-type and mutant roots. The
461 loss or the accumulation of root cap cell layers could alter not only the cap shape but also the
462 rigidity. A softer cap would deform more easily under an increase in medium strength, resulting
463 in the modification of its shape.

464 The difference in penetration abilities between mutant and wild-type roots may be assigned to
465 their different critical buckling forces. The *fez-2* non-penetrating roots mostly exhibited a step-
466 like shape even when subjected to a middle-strength medium, indicating that the low
467 resistance to buckling of *fez-2* roots did not allow them to deform the lower layer surface
468 sufficiently to prevent the root tip deviation. On the contrary, the higher buckling resistance of
469 *smb-3* roots allowed them to exert more axial stress on the lower layer surface and thus to
470 penetrate the strong layers more easily. When *smb-3* roots did not penetrate, they mostly
471 exhibited a curly phenotype, illustrating the fact that *smb-3* root tips deformed the lower layer
472 surface more than wild-type roots. The differences in the root critical buckling force between
473 the three *Arabidopsis* lines may be explained either by the differences in diameter or rigidity at
474 the buckling root zone, or by the differences in growth zone length (Kolb *et al.*, 2017). Altered
475 root cap shape or rigidity could not have influenced the resistance to buckling of the mutant
476 roots. Our observations of the mutant root phenotypes did not reveal any alterations in root
477 diameter, growth zone length or root hair initiation, suggesting that the root rigidity may be

478 altered negatively in *fez-2* and positively in *smb-3* mutant lines. We may hypothesize that the
479 increase in medium strength is perceived by root cap cells and that signal transduction in the
480 elongation zone triggers mechanisms leading to the regulation of tissue rigidity. For example,
481 root rigidity might be increased by auxin-dependent cell wall strengthening (Bengough *et al.*,
482 2011; Muratov and Baulin, 2015; Tsugama *et al.*, 2016). In *fez-2* roots, the loss of cap cell layers
483 may alter the mechanosensitivity and thus the regulation of cell wall extensibility in the
484 elongation zone in response to an increase in medium strength. The fact that the growth rate of
485 both *fez-2* penetrating and reorienting roots was not affected by medium strength consolidates
486 this hypothesis. Moreover, we observed that the second curvature of step-like shaped roots,
487 established through an active process, was of a lesser intensity in *fez-2* roots and of a greater
488 intensity in *smb-3* roots compared to wild-type roots. As *fez-2* and *smb-3* roots appear to have
489 an effective gravitropic response, the alteration in the curvature establishment may be the
490 result of a functional alteration in mutant root caps. The presence of a intact root cap with a
491 precise number of LRC and COL cell layers may be required to trigger the signal perception and
492 transduction processes within the root and thus to allow the root to respond to an increase in
493 medium strength.

494 **Conclusion**

495 During their progression in a soil, roots frequently face physical heterogeneities that they have
496 to displace by generating a sufficient mechanical force or circumvent by reorienting their
497 growth. The experimental approach presented here provides new insights into the role of the
498 root cap on root penetration and reorientation in response to medium strength. In two-layer
499 media, the roots adopted three main responses to an increase in medium strength: root
500 penetration in a brittle medium, root buckling without tip deviation leading to a curly
501 phenotype in a middle-strength medium, and root buckling followed by tip deviation leading to
502 a step-like phenotype in the strongest medium. The responses to medium strength were
503 altered in *fez-2* and *smb-3* mutant roots, which exhibit less and additional cap cell layers,
504 respectively. The alteration in the penetration ability, reduced in *fez-2* roots and enhanced in
505 *smb-3* roots was the result of altered resistance to buckling rather than of altered root cap

506 geometries. From these results arises the hypothesis that intact root cap layers are required to
507 trigger the root responses to medium strength.

508

509 **Supplementary data**

510 **Fig. S1. The two-layer Phytagel media 0.2-0.2, 0.2-0.3 and 0.2-0.5 were used to study the**
511 **responses of *Arabidopsis thaliana* roots to an increase in medium strength.**

512 **Fig. S2. Growth rate of reorienting roots of wild-type, *fez-2*, *smb-3 Arabidopsis thaliana* lines**
513 **in 0.2-0.5 two-layer medium**

514 **Fig. S3. Time-lapse movie of a reorienting wild-type root in the 0.2-0.3 two-layer medium**

515 **Fig. S4. Time-lapse movie of a reorienting wild-type root in the 0.2-0.5 two-layer medium**

516 **Fig. S5. Time-lapse movie of a reorienting *fez-2* root in the 0.2-0.2 two-layer medium**

517 **Fig. S6. Time-lapse movie of a reorienting *fez-2* root in the 0.2-0.3 two-layer medium**

518 **Fig. S7. Time-lapse movie of a reorienting *fez-2* root in the 0.2-0.5 two-layer medium**

519 **Fig. S8. Time-lapse movie of a reorienting *smb-3* root in the 0.2-0.5 two-layer medium**

520 **Acknowledgements**

521 We would like to thank Ben Scheres and Viola Willemsen (University of Utrecht, The
522 Netherlands) for the kind gifts of mutant lines, Nicole Brunel-Michac (Université Clermont
523 Auvergne, INRA, PIAF) for her help and advice on microscopy, Patricia Mabrut for English
524 editing (Université Clermont Auvergne). This research received financial support from the
525 French Space Agency (CNES) and by the recipient of INRA programs. J.R. has a doctoral grant of
526 the French National Ministry of Education and Research. H.C is supported by a Postdoctoral
527 grant from the Auvergne-Rhône Alpes Council with cofunding from FEDER. F. B. was supported
528 by a Postdoctoral grant from the CNES.

529 **References**

530 **Ahearne M, Yang Y, El Haj AJ, Then KY, Liu KK**. 2005. Characterizing the viscoelastic properties
531 of thin hydrogel-based constructs for tissue engineering applications. Journal of the Royal
532 Society Interface **2**, 455–463.

533 **Arnaud C, Bonnot C, Desnos T, Nussaume L**. 2010. The root cap at the forefront. Comptes
534 Rendus - Biologies **333**, 335–343.

535 **Barlow PW**. 2003. The Root Cap: Cell Dynamics , Cell Differentiation and Cap Function. Journal
536 of Plant Growth Regulation, 261–286.

537 **Bengough AG, Hans J, Bransby MF, Valentine TA**. 2009. PIV as a method for quantifying root
538 cell growth and particle displacement in confocal images. Microscopy Research and Technique
539 **73**, N27-36.

540 **Bengough AG, McKenzie BM, Hallett PD, Valentine TA**. 2011. Root elongation, water stress,
541 and mechanical impedance: a review of limiting stresses and beneficial root tip traits. Journal of
542 Experimental Botany **62**, 59–68.

543 **Bennett T, Sanchez-perez GF, Campilho A, Willemsen V, Snel B, Scheres B**. 2010. SOMBRERO ,
544 BEARSKIN1 , and BEARSKIN2 Regulate Root Cap Maturation in Arabidopsis. The Plant Cell **22**,
545 640–654.

546 **Bennett T, van den Toorn A, Willemsen V, Scheres B**. 2014. Precise control of plant stem cell
547 activity through parallel regulatory inputs. Development **141**, 4055–4064.

548 **Bizet F, Bengough AG, Hummel I, Bogeat-Triboulot M-B, Dupuy LX**. 2016. 3D deformation field
549 in growing plant roots reveals both mechanical and biological responses to axial mechanical
550 forces. Journal of Experimental Botany **67**, 5605–5614.

551 **Chauvet H, Pouliquen O, Forterre Y, Legué V, Moulia B**. 2016. Inclination not force is sensed by
552 plants during shoot gravitropism. Scientific Reports **6**, 1–8.

553 **Colombi T, Braun S, Keller T, Walter A**. 2017*a*. Artificial macropores attract crop roots and

enhance plant productivity on compacted soils. Science of the Total Environment **574**, 1283–1293.

Colombi T, Kirchgessner N, Walter A, Keller T. 2017*b*. Root Tip Shape Governs Root Elongation Rate under increased soil strength. Plant Physiology **174**, 2289–2301.

Hanaor DAH, Gan Y, Einav I. 2015. Contact mechanics of fractal surfaces by spline assisted discretisation. International Journal of Solids and Structures **59**, 121–131.

Iijima M, Barlow PW, Bengough AG. 2003*a*. Root cap structure and cell production rates of maize (Zea mays) roots in compacted sand. New Phytologist **160**, 127–134.

Iijima M, Higuchi T, Barlow PW, Bengough AG. 2003*b*. Root cap removal increases root penetration resistance in maize (Zea mays L .). Journal of Experimental Botany **54**, 2105–2109.

Jin K, Shen J, Ashton RW, Dodd IC, Parry MAJ, Whalley WR. 2013. How do roots elongate in a structured soil? Journal of Experimental Botany **64**, 4761–4777.

Kolb E, Legué V, Bogeat-Triboulot M-B. 2017. Physical root – soil interactions. Physical Biology **14**.

Kumpf RP, Nowack MK. 2015. The root cap: a short story of life and death. Journal of Experimental Botany **66**, 5651–5662.

Massa GD, Gilroy S. 2003. Touch modulates gravity sensing to regulate the growth of primary roots of Arabidopsis thaliana. Plant Journal **33**, 435–445.

Materechera SA, Alston AM, Kirby JM, Dexter AR. 1992. Influence of root diameter on the penetration of seminal roots into a compacted subsoil. Plant and Soil **144**, 297–303.

Muratov A, Baulin VA. 2015. Biophysical Chemistry Mechanism of dynamic reorientation of cortical microtubules due to mechanical stress. Biophysical Chemistry **207**, 82–89.

Ruiz S, Straub I, Schymanski SJ. 2016. Experimental Evaluation of Earthworm and Plant Root Soil Penetration – Cavity Expansion Models Using Cone Penetrometer Analogs. Vadose Zone

578 Journal.

579 **Sato EM, Hijazi H, Bennett MJ, Vissenberg K, Swarup R**. 2015. New insights into root
580 gravitropic signalling. Journal of Experimental Botany **66**, 2155–2165.

581 **Schiavi A, Cuccaro R, Troia A**. 2016. Strain-rate and temperature dependent material
582 properties of Agar and Gellan Gum used in biomedical applications. Journal of the Mechanical
583 Behavior of Biomedical Materials **53**, 119–130.

584 **Silverberg JL, Noar RD, Packer MS, Harrison MJ, Henley CL, Cohen I, Gerbode SJ**. 2012. 3D
585 imaging and mechanical modeling of helical buckling in Medicago truncatula plant roots.
586 Proceedings of the National Academy of Sciences **109**, 16794–16799.

587 **Tsugama D, Liu S, Takano T**. 2016. The bZIP Protein VIP1 Is Involved in Touch Responses in.
588 Plant Physiology **171**, 1355–1365.

589 **Vollsnes a. V., Futsaether CM, Bengough a. G**. 2010. Quantifying rhizosphere particle
590 movement around mutant maize roots using time-lapse imaging and particle image
591 velocimetry. European Journal of Soil Science **61**, 926–939.

592 **Willemsen V, Bauch M, Bennett T, Campilho A, Wolkenfelt H, Xu J, Haseloff J, Scheres B**. 2008.
593 Article The NAC Domain Transcription Factors FEZ and SOMBRERO Control the Orientation of
594 Cell Division Plane in Arabidopsis Root Stem Cells. Developmental Cell **15**, 913–922.

595 **Yamamoto C, Sakata Y, Taji T, Baba T, Tanaka S**. 2008. Unique ethylene-regulated touch
596 responses of Arabidopsis thaliana roots to physical hardness. Journal of Plant Research **121**,
597 509–519.

598 **Yan J, Wang B, Zhou Y**. 2017. A root penetration model of Arabidopsis thaliana in phytagel
599 medium with different strength. Journal of Plant Research **130**, 941–950.

600

601 **Tables**

602 **Table 1. Penetration ability of Arabidopsis wild-type (Col-O), *fez-2*, and *smb-3* loss-of-function**
603 **mutant primary roots in two-layer media.** Penetration ability is represented by the percentage
604 of roots that were able to penetrate 0.2%, 0.3% and 0.5% lower layers. For each genotype and
605 condition, 6 replicates of 10 roots were observed 8 days after germination. The values indicate
606 the average percentage over the six replicates, + or – SD. Letters indicate means significantly
607 different with P<0.05 (two-way ANOVA with Tukey test)

608

609 **Figure legends**

610 **Fig. 1. Mechanical properties of Phytagel growth media illustrated by the determination of**
611 **Elastic modulus (A-C) and by penetrometer capacity (D-F).** (A) Representation of Phytagel cube
612 placed between the two plates of the testing machine (Instron). (B) Stress-strain curves
613 resulting from compressive tests performed for medium cubes of Phytagel concentration
614 ranging from 0.2% to 1.2%. (C) The Elastic modulus E was estimated using the slope of the
615 linear portion of the curve. The circles are real data obtained for each Phytagel concentration,
616 squares are means, n=4. (D-F) Penetrometer assays to determine mechanical resistance of the
617 lower layer surface in two-layer media. (D) Representation of the needle progression in a 0.2-
618 0.5 two-layer medium in the mechanical testing machine. (E) Measurement of force during the
619 penetration of the needle in the lower medium layer of 0.2%, 0.3% and 0.5% Phytagel. The
620 displacement 0 corresponds to the first contact between the needle tip and the lower layer
621 surface (F) Penetrometer resistance of the lower layer surface of 0.2%, 0.3% or 0.5 % Phytagel.
622 Circles are real data, squares are means, n=4.

623 **Fig. 2. Root shape of wild-type, *fez-2* and *smb-3 Arabidopsis thaliana* root tip**

624 (A-D) Representative Confocal microscope images of Ps-PI stained Col-0 (A), *fez-2* (B) and *smb-3*
625 (C) 5 day-old roots. Asterisks indicate the quiescent center. White bar = 100 µm. (D1)
626 Representation of the root tip section used to measure root radius at the quiescent center (R_R)
627 and root length from the quiescent center to the root tip extremity (L_R). (D2) The root tip area
628 measured in D1 was compared to the areas of a triangle and a rectangle of the same

629 dimensions (L_R and R_R) to obtain the Sharpness Index (SI) of the root tip. (E) Diameter of Col-0,
630 *fez-2* and *smb*-3 roots at the quiescent center (filled markers) and at 500 µm from the root tip
631 extremity, in the elongation zone (empty markers). Circles are real values and squares are
632 means, n=8 (F) SI of Col-0, *fez-2, smb-3* root tips. The SI lies between 0 - value corresponding to
633 a triangle - and 1- value corresponding to a rectangle. Circles are real values and squares are
634 means, n=8. (G) Root growth rate of Col-0, *fez-2, smb-3* roots growing in compliant one-layer
635 0.2% Phytagel-medium. Circles are real values and squares are means, n=12. Letters indicate
636 means significantly different with P<0.05 (ANOVA with Tukey test)

637

638 **Fig. 3. Growth rate of penetrating roots of Col-0, *fez-2, smb-3 Arabidopsis thaliana* lines in**
639 **two-layer media**

640 (A-C) Root growth rate of Col-0 (A), *fez-2* (B), *smb-3* (C) roots which penetrated a compliant
641 lower medium layer (0.2% Phytagel). (D-F) Root growth rate of Col-0 (D), *fez-2* (E), *smb-3* (F)
642 roots which penetrated a middle strength lower medium layer (0.3% Phytagel). For all graphs,
643 circles are real values and lines are mean, 6<n<10.

644 **Fig. 4. Critical buckling force of Col-0, *fez-2* and *smb-3* roots**

645 (A) Schematic example of a root tip growing against a 0.3% lower layer surface of elastic
646 modulus E= 7.6 kPa. The gray curve represents the shape of the lower layer surface just before
647 root curvature initiation. d is the maximal interface displacement. R is the radius of the root tip
648 in contact with the surface.

649 (B) Shapes of the lower layer surface of Elastic modulus E = 7.6 kPa deformed by Col-0, *fez-2*
650 and *smb-3* root tips just before their curvature initiation. Lines are means, n=10. Dashed lines
651 correspond to the initial shape of the lower layer surface.

652 (C) Evaluation of the critical force Fcrit that the Col-0, *fez*-2 and *smb-3* roots were able to exert
653 on the lower layer surface before reorienting. Fcrit was computed according to the equation
654 depending on root tip radius R, on the maximal displacement d and on the elastic modulus of

655 the lower layer E. (n=10). Letters indicate means significantly different with P<0.05 (ANOVA
656 with Tukey test)

657 **Fig. 5. Spatiotemporal characterization of *Arabidopsis* Col-0 root reorientation in two-layer**
658 **media.** (A) Representative Col-0 root penetration into a compliant lower layer (0.2% Phytagel).
659 Images represent the root 2 h before contact with the lower layer surface and 0 h, 3 h and 6 h
660 after contact. (A1) Skeleton of the root during the penetration. (B) Representative Col-0 root
661 response to contact with a 0.3% lower layer at 0 h, 5 h, 10 h and 15 h after contact. This
662 response is called curly phenotype. (B1) Skeleton of the root during the beginning of its
663 reorientation, from 4 h before contact to 6 h after contact. (C) Representative wild-type root
664 response to contact with a 0.5% lower layer at 0 h, 3 h, 8 h and 15 h after contact. (C1) Skeleton
665 of the root during its reorientation, from 4 h before the contact to 14 h after the contact. White
666 bars correspond to 500 µm. Red arrows indicate lower layer surface (D-F) Spatiotemporal
667 analyses of a root penetrating a compliant lower layer (D), a root reorienting in response to
668 middle strength lower layer (E) and a root reorienting in response to stiff lower layer (F). For 3D
669 graphs, root length as a function of time is presented. The colors represent curvature intensity:
670 negative for right-handed curvatures and positive for left-handed curvatures. The green color
671 corresponds to the straight zones of the roots. The dashed lines indicate the contact.

672 **Fig. 6. Spatiotemporal characterization of *fez-2* root reorientation in two-layer media**

673 (A-B) Squeletton (A) and spatio-temporal analysis (B) of a root reorienting after contact with a
674 0.2% lower layer. (C-D) Skeleton (C) and spatio-temporal analysis (D) of a root reorienting after
675 contact with 0.3% lower layer. (E-F) Squeletton (E) and spatio-temporal analysis (F) of a root
676 reorienting after contact with a 0.5% lower layer. Dashed lines indicate the contact between
677 root tip and lower layer surface.

678 **Fig. 7. Spatiotemporal characterization of *smb-3* root reorientation in two-layer media**

679 (A-B) Squeletton (A) and spatio-temporal analysis (B) of a root reorienting after contact with a
680 0.3% lower layer. (C-D) Skeleton (C) and spatio-temporal analysis (D) of a root reorienting
681 through waves formation after contact with a 0.5% lower layer. (E-F) Squeletton (E) and spatio-

682 temporal analysis (F) of a root reorienting through a step-like phenotype after contact with a
683 0.5% lower layer. Dashed lines indicate the contact between root tip and lower layer surface.

Genotype	Two-layer medium		
Concentrations of the two layer media (% phytagel)	0.2-0.2	0.2-0.3	0.2-0.5
Rupture Force (N)	0.032 ± 0.004	0.054 ± 0.008	0.11 ± 0.009
Col-0	100.00 ± 0.00 [a]	60.00 ± 3.65 [c]	1.67 ± 1.67 [e]
fez-2	83.33 ± 4.94 [b]	28.33 ± 3.07 [d]	0.00 ± 0.00 [e]
smb-3	100.00 ± 0.00 [a]	80.00 ± 5.16 [b]	18.33 ± 4.77 [d]

Table 1. Penetration ability of Arabidopsis wild-type (Col-O), *fez-2*, and *smb-3* loss-of-function mutant primary roots in two-layer media.

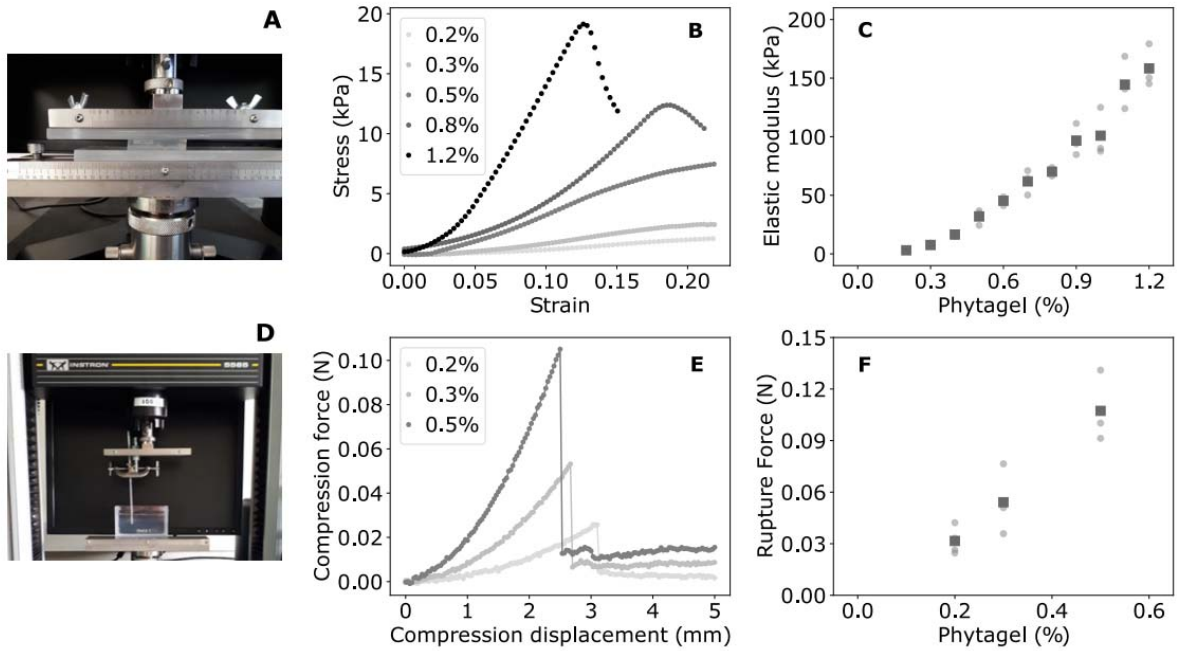

Fig. 1. Mechanical properties of Phytagel media.

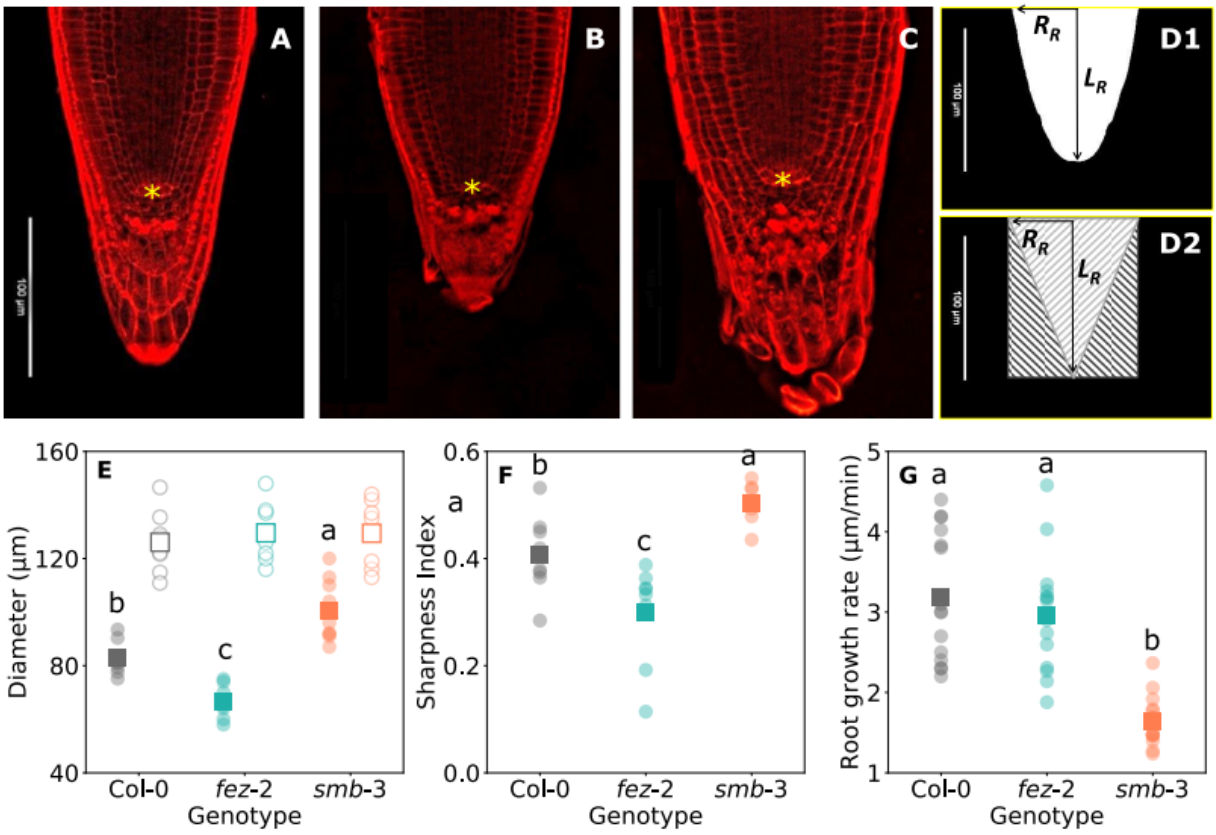

Fig. 2. Phenotypes of Col-0, *fez-2* and *smb-3* roots.

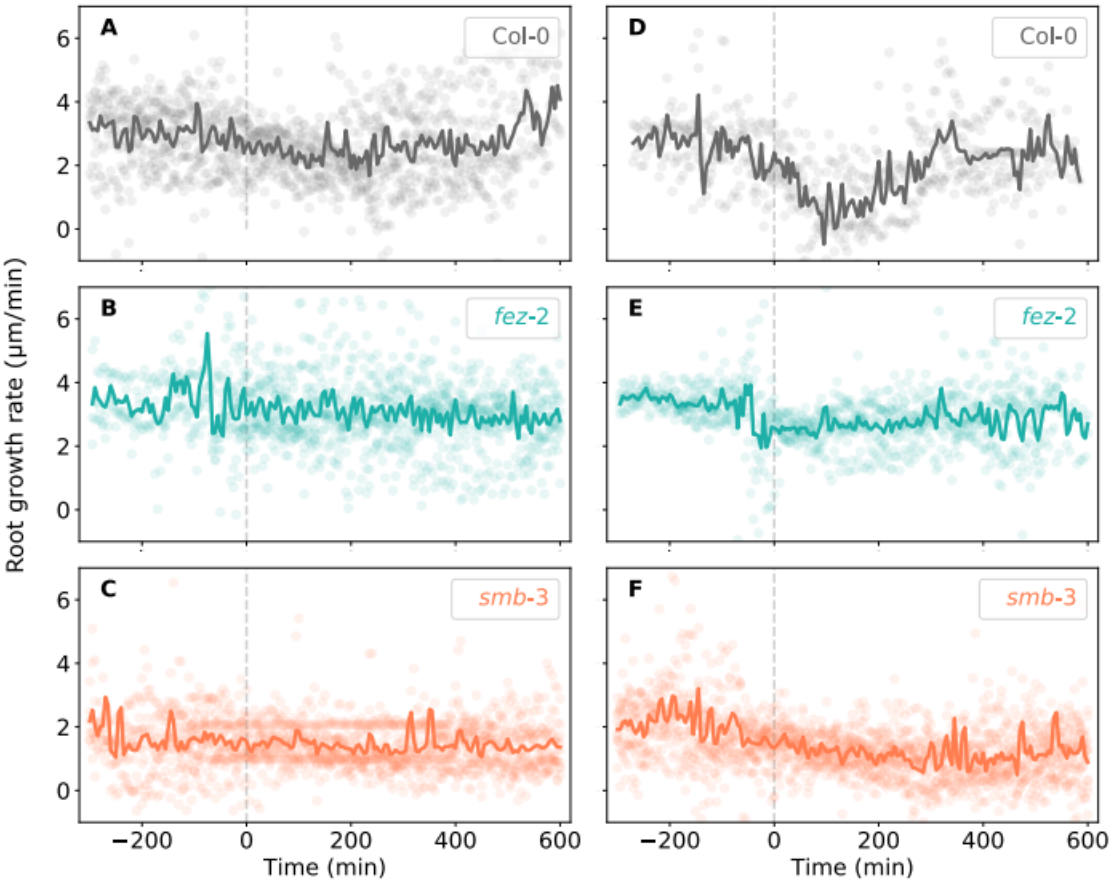

Fig. 3. Root growth rate of Col-0, *fez-2*, *smb-3* Arabidopsis lines in two-layer media

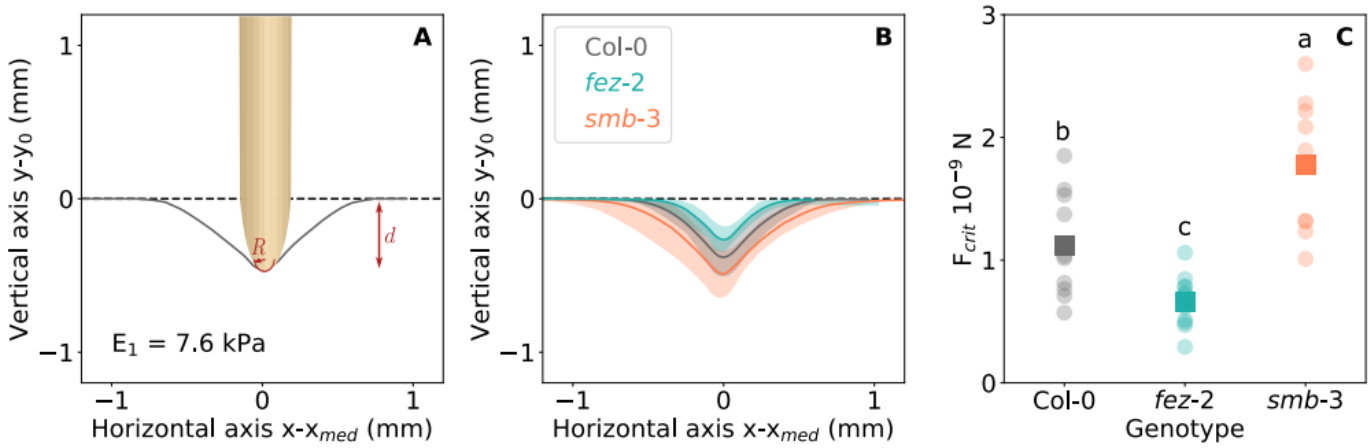

Fig. 4. Critical buckling force of Col-0, *fez-2* and *smb-3* roots.

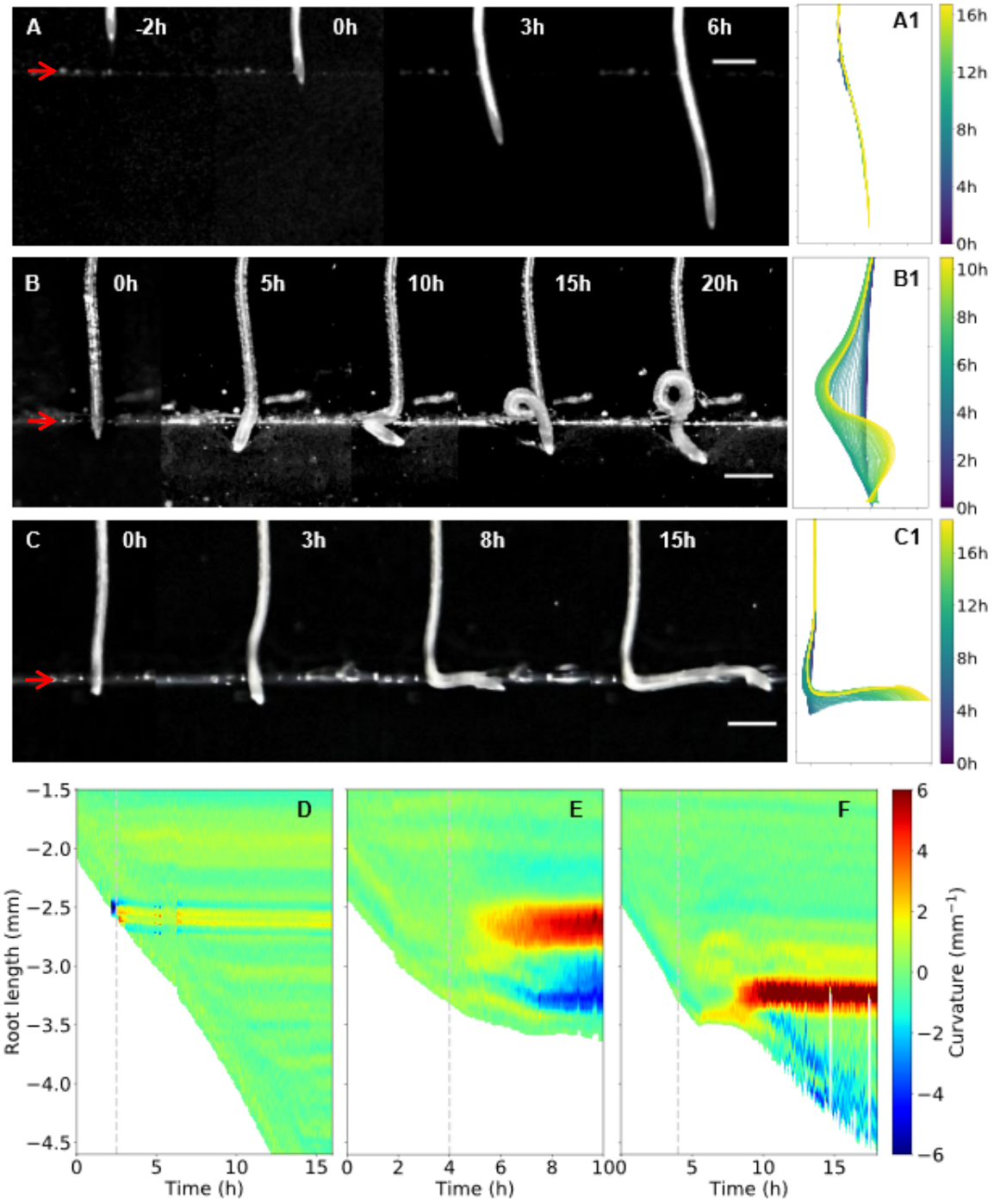

Fig. 5. Spatiotemporal characterization of *Arabidopsis* Col-0 root reorientation in two-layer media.

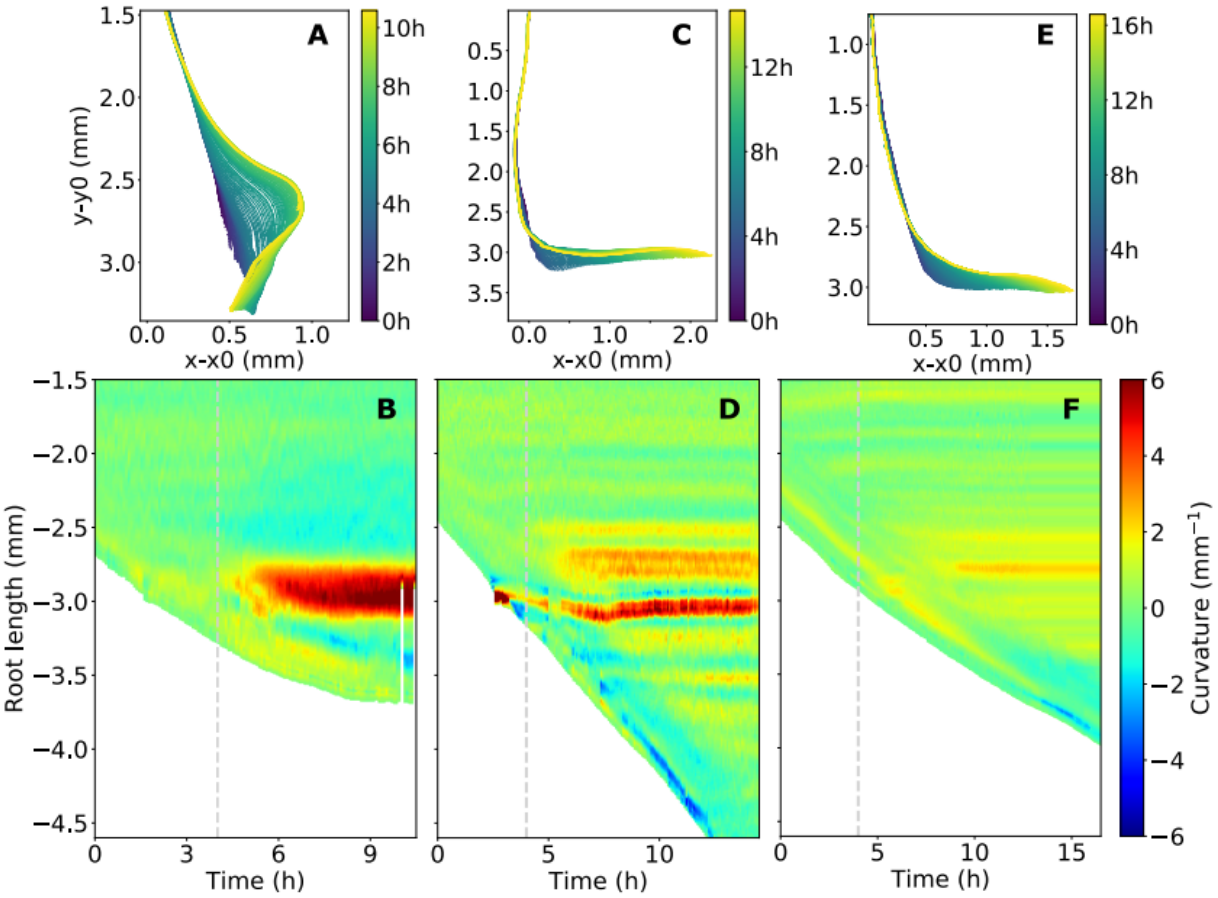

Fig. 6. Spatiotemporal characterization of *fez-2* root reorientation in two-layer media.

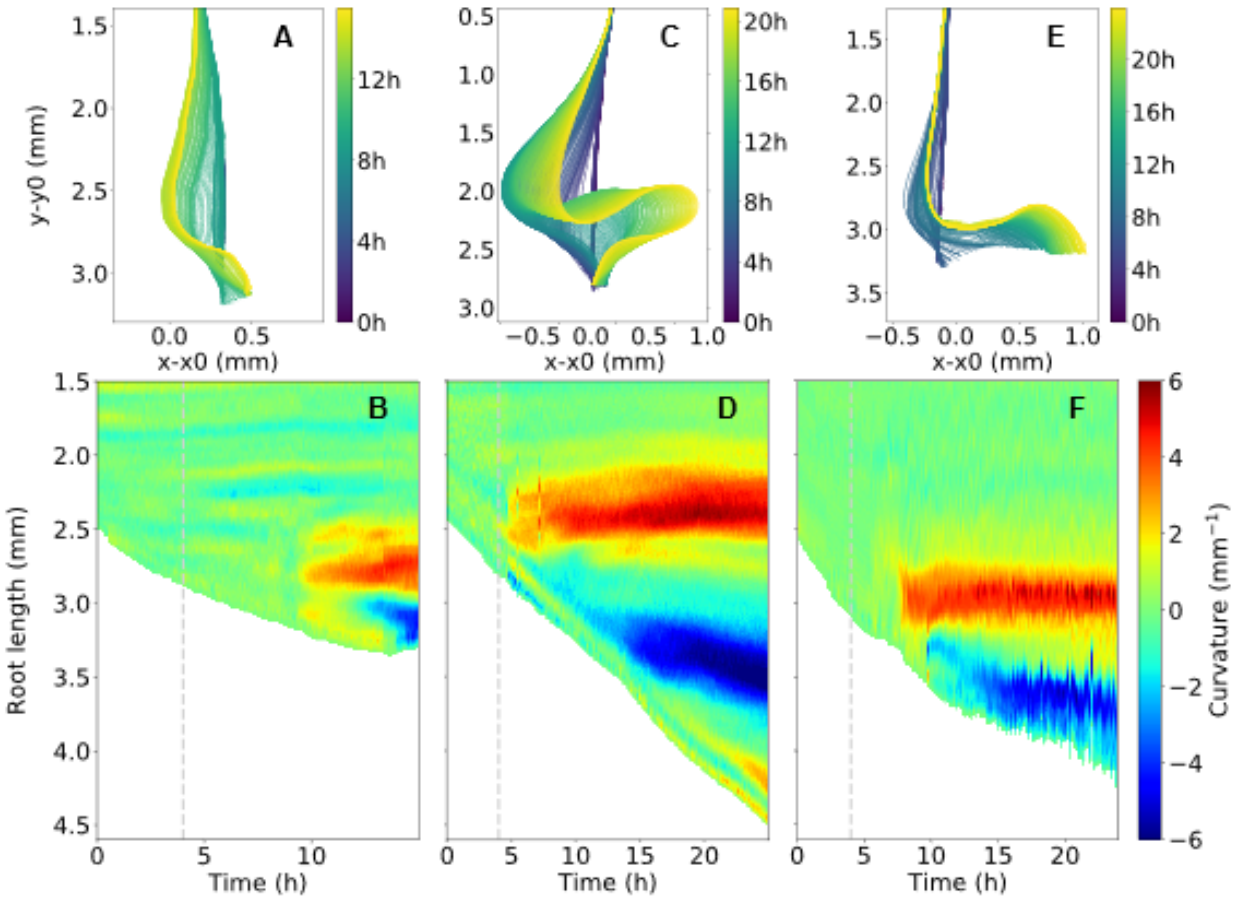

Fig. 7. Spatiotemporal characterization of *smb-3* root reorientation in two-layer media.